

## Understanding macrophysical outcomes of microphysical choices in simulations of shallow cumulus convection

**Björn STEVENS**

*Department of Atmospheric and Oceanic Sciences, University of California Los Angeles,  
Los Angeles, California, USA*

and

**Axel SEIFERT**

*Deutscher Wetterdienst, Offenbach, Germany*

*(Manuscript received 1 August 2007, in final form 25 April 2008)*

### Abstract

The sensitivity of simulations of shallow cumulus convection to their microphysical representation is explored, with a focus on the parameter space spanned by two common bulk schemes (Seifert and Beheng, SB, versus Khairoutdinov and Kogan, KK). Large-eddy simulation, simple models, and *a priori* analysis of the underlying microphysical equations are used as the basis for our study. The simulations are initialized using data derived from the Rain in Cumulus Over the Ocean (RICO) field study. Simulated clouds depths range between two and three kilometers. Microphysical sensitivities can largely be rationalized based on the behavior of simpler models. In particular a parcel model consisting of auto-conversion and accretion acting on a parcel condensing water at a fixed rate provides useful insight into the behavior of the microphysical schemes in the full simulation. To a first approximation the number concentration simply selects the cloud depth at which rain begins to develop, with different schemes predicting different cloud depths. Because of the interaction of auto-conversion and accretion the dependence of this cloud depth on cloud-droplet number concentration is considerably reduced from what would be deduced by an examination of auto conversion alone—suggesting a somewhat diminished role for the regulation of rain by the atmospheric aerosol. Dynamic feedbacks, such as the tendency for non-precipitating clouds to deepen more readily, can further dampen (and even reverse) the expected sensitivity of rain-rate on droplet number concentrations. Our analysis suggests that the commonly assumed exponential distribution for rain drops can strongly distort the sedimentation process in two moment microphysical schemes and that processes such as self-collection and drop break-up can not be neglected for shallow cumulus convection.

### 1. Introduction

The emergence of convection permitting simulations in both global climate (Tomita et al. 2005) and

numerical weather prediction models<sup>1</sup> is contributing to a shift in emphasis away from convective parameterization and toward cloud-microphysical parameterizations and boundary layer processes. Indeed the ability of even poorly resolved convection permitting simulations to provide a conceptu-

---

Corresponding author: Björn Stevens, Max-Planck-Institute for Meteorology, Department "Atmosphere in the Earthsystem", Bundesstr. 53, 20146 Hamburg, Germany

E-mail: bjoern.stevens@zmaw.de

©2008, Meteorological Society of Japan

---

<sup>1</sup> The DWD Lokal (LMK) model has been run at an operational resolution of 2.8 km since August 2006 Baldauf et al. (2007)

ally simpler framework for coupling otherwise disparate sub-gridscale processes such as turbulence, radiation, clouds, chemistry and precipitation, has been a major motivation in their development. These developments and the emergence of new global data sets capable of providing cloud microphysical information serves as the backdrop for our present study, wherein we investigate the sensitivity of large-eddy simulations of shallow cumulus convection to the representation of cloud microphysical processes.

Our focus will be on the macrophysical outcomes of microphysical choices. Does the behavior of cloud fields reflect, in a simple way, the assumptions made at the process level of the microphysical model? For instance, do simulations based on more efficient auto-conversion schemes necessarily rain more, or are such effects controlled by other processes? To the extent one can draw a link between assumptions made at the microphysical level, and their macrophysical outcomes, then there is hope for constraining microphysical processes, using statistical data on the cloud scale, such as provided by radar. As such this study should be seen as a prelude to data based inquiries which aim to attribute macrophysical behavior to microphysical processes.

In some sense our work strives to fill the gap between the proliferation of papers devoted to the development of simplified models (Feingold et al. 1994; Khairoutdinov and Kogan 2000; Seifert and Beheng 2001; Morrisson and Grabowski 2007, among others), and the use of large-eddy simulation to study aerosol-cloud interactions from the perspective of climate (e.g., Kogan et al. 1995; Stevens et al. 1998; Jiang and Cotton 2000; Ackerman et al. 2004; Xue et al. 2008). The former line of research emphasizes the fidelity of models of specific processes to *a priori* information, for instance as provided by more accurate integrations of the underlying equations, or available data (e.g., Wood 2005). It is difficult to develop a balanced view of microphysical processes in such an approach, as the important properties of a microphysical scheme may only emerge through the interaction of the myriad cloud microphysical processes with each other and with cloud dynamical processes. Although the use of non-parametric representations of the cloud may seem to obviate such issues, they do so at considerable computational cost, and often at the expense of an adequate representation of cloud dynamical processes. This is most cer-

tainly the case for detailed microphysical schemes coupled to very coarse resolution convection permitting models, such as might be expected from the emerging generation of convection permitting simulations for climate and weather.

The outline of our investigation is as follows. In Section 2 we introduce the case being simulated, the model and microphysical parameterizations that underly the simulations, as well as an overview of the simulation methodology. Section 3 presents the simulations, while Section 4 interprets the simulations in light of the structure of the underlying microphysical model being used. These two sections show that although the microphysical assumptions can significantly impact the cloud and microphysical structure of the simulations, many of these effects can be readily understood in terms of the underlying structure and assumptions of the microphysical model. Section 5 summarizes our findings and outlines some avenues for future investigation.

## 2. Methodological background

### a. Large-Eddy Simulation Code

The basic code is the same as described in Stevens et al. (2005b), it solves prognostic equations for the three components of the velocity ( $u, v, w$ ), and variables specifying the thermodynamic state, on a regular three-dimensional Cartesian mesh. The thermodynamic coordinates are the total water mixing ratio,  $r_t$  and the liquid-water potential temperature,  $\theta_l$ . Cloud and microphysical processes are represented following the procedures described by Savic-Jovicic and Stevens (2008). This involves the solution of two additional prognostic equations: one for the mass mixing ratio of rain water,  $r_r$ , the other for mass specific number of rain-water drops  $n_r$ . The cloud water mixing ratio,  $r_c$  is diagnosed as

$$r_c = \max(0, r_t - r_r - r_s), \quad (1)$$

where  $r_s$  is the saturation mixing ratio and is diagnosed from the basic state pressure and  $\theta_l$ . This approach is facilitated by assuming that the surface area of cloud droplets far exceeds that of rain drops and thus vapor deposition to hydrometeors can be carried entirely by the cloud-droplet mode. Because  $\theta_l$  depends on the total condensate present in the domain, this defines an implicit equation for  $r_c$  which we solve iteratively. Cloud number mixing ratio,  $N_c$ , is fixed as a parameter, i.e., we do not attempt to model the aerosol or cloud condensation

nuclei (CCN) budget, nor do we explicitly predict activation/nucleation.

In the anelastic approximation, with  $\rho$  denoting the ambient fluid density, the prognostic equation for the microphysical quantities take the form

$$\begin{aligned} \frac{\partial \psi}{\partial t} + \frac{1}{\rho} \nabla \cdot (\mathbf{u} \rho \psi - \rho K_\psi \nabla \psi) \\ = -\frac{1}{\rho} \frac{\partial}{\partial z} (\rho w_\psi \psi) + \mathcal{K}_\psi + \mathcal{T}_\psi, \end{aligned} \quad (2)$$

where  $\psi$  denotes a scalar field, in our case  $\psi \in \{n_r, r_r\}$ . The terms on the lhs represent dynamic processes, and  $K_\psi$  is the eddy diffusivity of  $\psi$  which we set to  $K_h$  the eddy diffusivity of heat. The rhs terms represent different classes of microphysical processes. From left to right these are: (i) sedimentation, with terminal velocity  $w_\psi$ ; (ii)  $\mathcal{K}_\psi$ , the transformation of  $\psi$  due to kinetic processes; and (iii)  $\mathcal{T}_\psi$ , the transformation associated with thermodynamic processes, which given our assumption that condensation is carried entirely by the cloud droplets, includes only evaporation. Note that the microphysical literature often speaks of kinetic effects in terms of molecular kinetics; here we use *kinetic* to describe microphysical transformations arising from the interactions among drops.

For bulk microphysical models the microphysical sources depend on assumptions made in the formulation of the model. Ideally, given the underlying microphysical equations one needs only to make an assumption on the distribution to derive a bulk microphysical model. Practically, many microphysical schemes are derived less formally which means that the assumptions or approximations made in representing various terms usually cannot be consistently related to a single underlying assumption.

In this work we explore the space spanned by two microphysical schemes. The first was developed by Seifert and Beheng (2001, hereafter SB) from asymptotic arguments and detailed microphysical modeling in simplified dynamical contexts. The second was developed by Khairoutdinov and Kogan (2000) using a pseudo-empirical approach centered around large-eddy simulations of stratocumulus with a bin-microphysical representation. SB and KK are similar in that they represent kinetic effects given a two moment (mass and number) representation of the droplet distribution. Although both schemes provide evolution equations for the cloud-droplet number mixing ratio,

the present implementation is based on an equilibrium cloud water (fixed cloud-droplet number) assumption, thereby reducing the number of additional prognostic equations that must be carried by the model by two. The microphysical modeling we describe here differs from Savic-Jovicic and Stevens (2008) both in terms of its inclusion of the KK scheme, but also in that the present work implements a modified representation of sedimentation, a larger cut-off diameter between cloud droplets and rain drops (80 instead of 50  $\mu\text{m}$ ), and a more general treatment of evaporation effects. The numerical implementation of the model also differs slightly. Relevant technical details are provided in an appendix.

*i. SB*

The SB model adopts the master function approach. Let  $f(D) dD$  describe the number of liquid drop/droplets per kg of air per drop(let) diameter interval  $dD$ , i.e.,  $f(D)$  has units of  $\text{kg}^{-1} \text{m}^{-1}$ . The nature of stochastic-coalescence supports the decomposition of  $f(D)$  into two separated distributions, such that  $f(D) = f_c(D) + f_r(D)$ , with  $f_c \gg f_r$  for  $D < D_*$  and  $f_c \ll f_r$  otherwise, with the separation diameter  $D_* = 80 \mu\text{m}$ .

We write the density distribution of rain-drop number mixing ratio ( $n_r$ ) as a Gamma distribution such that

$$f_r(D) = n_r \left( \frac{D}{D_b} \right)^\mu \frac{\exp(-D/D_b)}{D_b \Gamma(\mu + 1)}, \quad (3)$$

which introduces  $\mu$  the shape parameter, and  $D_b$  a size parameter.  $\Gamma$  is the Gamma function. The number concentration is thus just  $\rho n_r$ . SB originally set  $\mu = 0$ , in this case  $D_b$  can be interpreted as the mean diameter. Here motivated by ongoing work examining evaporation (Seifert 2008), and the recent study of Milbrandt and Yau (2005), the formulation is generalized to allow  $\mu > 0$ . Given this formulation, the moments describing the rain-water number and mass-mixing ratio are respectively:

$$\begin{aligned} n_r &= \int_0^\infty f_r(D) dD \quad \text{and} \\ r_r &= \rho_l \frac{\pi}{6} \int_0^\infty D^3 f_r(D) dD, \end{aligned} \quad (4)$$

where  $\rho_l$  is the density of liquid water. Given  $\mu, D_b$  can be related to these moments by noting that

$$D_p = \left[ \frac{6r_r}{\pi \rho_l n_r (\mu + 3)(\mu + 2)(\mu + 1)} \right]^{1/3} \quad (5)$$

In two-moment schemes  $\mu$  usually enters as a parameter, although it can be allowed to vary as a function of the other moments. For instance, for many of our simulations we diagnose

$$\mu = 10\{1 + \tanh[1200(D_m - 0.0014)]\}, \quad (6)$$

where

$$D_m = \left[ \frac{r_r}{n_r} \left( \frac{6}{\rho_l \pi} \right) \right]^{1/3}, \quad (7)$$

is the mean volume (or mass) diameter. We note that as  $D_m \rightarrow 0$ ,  $\mu$  approaches zero, and  $f_r$  approaches an exponential distribution. Thus the parameterization (6) has the effect of narrowing the distribution as the average drop size increases, so doing has been argued to improve the representation of sedimentation processes.

Neglecting the effects of variable air density (which can be justified for shallow clouds) the SB model is as follows

$$\mathcal{K}_r^{(sb)} = a_{sb} \frac{r_c^4}{N_c^2} \phi_{cc}(\varepsilon) + b_{sb} r_c \phi_{cr}(\varepsilon), \quad (8)$$

$$\mathcal{K}_{n_r}^{(sb)} = \frac{6}{\rho_l D_*^3 \pi} \left[ a_{sb} \frac{r_c^4}{N_c^2} \phi_{cc}(\varepsilon) \right] - b_{sb} n_r r_r \beta(D_m). \quad (9)$$

Here  $a_{sb}$  is a constant (Table 1) which is derived using the Long (1974) kernel for collection and incorporates the assumed shape of the cloud-droplet distribution. This kernel has the attractive feature of eliminating any dependence of accretion on  $\mu$ . Collisional breakup of rain drops, which includes rebound effects, i.e., all effects of coalescence efficiencies less than unity, is represented by a linear decrease of the self-collection rate, so that

$$\beta(D_m) = \begin{cases} 1 & D_m \leq 0.3 \times 10^{-3} \text{ m} \\ 1000D_m - 1.1 & D_m > 0.3 \times 10^{-3} \text{ m} \end{cases} \quad (10)$$

Non-equilibrium effects in auto-conversion and accretion are respectively modeled by the terms

$$\begin{aligned} \phi_{cc}(\varepsilon) &= 1 + 600 \frac{\varepsilon^{0.68} (1 - \varepsilon^{0.68})^3}{1 - \varepsilon} \quad \text{and} \\ \phi_{cr}(\varepsilon) &= \left( \frac{\varepsilon}{\varepsilon + 5 \times 10^{-4}} \right)^4, \end{aligned} \quad (11)$$

with

$$\varepsilon = \frac{r_r}{r_c + r_r}. \quad (12)$$

Here  $\varepsilon$  is to be thought of as a non-dimensional time that measures the progression of the cloud water into rain water. It introduces an  $r_r$  dependency into the parameterization of auto-conversion which attempts to model the effects of droplet spectral ripening (Cotton 1972; Lüpkes et al. 1989), its presence complicates comparisons between SB and other parameterizations of auto-conversion.

Sedimentation is determined through a specification of the sedimentation velocities, which we write as

$$\begin{aligned} w_{n_r} &\equiv \frac{1}{n_r} \int_0^\infty W_\infty(D) f(D) dD \\ &= 9.65 [1 - c_{sb} (1 + 600D_p)^{-(\mu+1)}], \end{aligned} \quad (13)$$

$$\begin{aligned} w_r &\equiv \frac{1}{n_r D_m^3} \int_0^\infty W_\infty(D) D^3 f(D) dD \\ &= 9.65 [1 - c_{sb} (1 + 600D_p)^{-(\mu+4)}], \end{aligned} \quad (14)$$

where  $W_\infty$  is the terminal velocity, which depends only on the size of the drop and is implicitly defined based on these relations.  $c_{sb}$  is a constant, whose value along with other constants used by the scheme are given in Table 1.

Overall our formulation differs from the original proposal of SB both through the inclusion of  $\mu$  effects in the representation of the fall-velocities and the representation of rain-drop break-up.

ii. KK

The KK Model is formulated as

$$\mathcal{K}_r^{(kk)} = a_{kk} \left( \frac{r_c}{N_c} \right)^{17/9} + b_{kk} (r_c r_r)^{1.15}, \quad (15)$$

$$\mathcal{K}_{n_r}^{(kk)} = \frac{6}{\rho_l D_*^3 \pi} \left[ a_{kk} \left( \frac{r_c}{N_c} \right)^{17/9} \right], \quad (16)$$

and the sedimentation velocities are specified as

$$w_{n_r} = 3500D_m - 0.1 \quad \text{and} \quad w_r = 6000D_m - 0.2. \quad (17)$$

The KK model is simpler as compared to SB, in that kinetic effects are not allowed to play as significant a role in the evolution of  $n_r$ , and because the two terms comprising  $\mathcal{K}_r$ , typically associated with auto-conversion and accretion respectively,

Table 1. Constants for Microphysical Models.

Constant	Values	Unites
$a_{sb}$	$1.4085 \times 10^{19}$	$\text{kg}^{-2} \text{s}^{-1}$
$b_{sb}$	5.78	$\text{s}^{-1}$
$c_{sb}$	1.015113	-
$a_{kk}$	$6.12 \times 10^{12}$	$\text{kg}^{-17/9} \text{s}^{-1}$
$b_{kk}$	67.	$\text{s}^{-1}$

do not allow for the aging of the droplet-spectrum, something which the  $\phi$  terms in SB attempts to parameterize. KK's neglect of self collection and breakup is consistent with its formulation based on simulations of drizzling stratocumulus. Here it merits emphasizing that the designers of the KK model did not intend their model to be used in situations (such as we propose) where such effects may become important.

*b. Initial data*

The initial thermodynamic data consists of horizontally homogeneous, piece-wise linear profiles of  $\theta_i$  and  $r_i$ : the total-water mixing ratio,  $r_i$ :

$$\theta_i(z) = \begin{cases} 297.9 & z < 740 \\ 297.9 + 19.1(\frac{z-740}{3260}) & 740 < z \end{cases}$$

$$r_i(z) = \begin{cases} 16.0 - 2.2(\frac{z}{740}) & z \leq 740 \\ 13.8 - 9.4(\frac{z-740}{2520}) & 740 < z < 3260, \\ 4.4 - 0.8(\frac{z-3260}{740}) & 3260 < z \end{cases} \quad (18)$$

with  $z$  the height in meters. The initial wind profile is assumed to be geostrophically balanced with uniform shear only in the zonal wind component, so that  $u = -9.9 + 2 \times 10^{-3} z$  and  $v = -3.8 \text{ m s}^{-1}$ . The simulations are performed on an  $f$ -plane with value of  $f$  corresponding to  $18^\circ\text{N}$ . The surface boundary condition is set to a fixed temperature of 299.8 K, as on the scale of our domain the surface temperature gradients required, by thermal wind, to balance the mean shear in the zonal wind, are entirely negligible. The surface pressure is set to 1015.4 hPa, and the lower surface is assumed to be saturated, which given the surface pressure determines  $r_i$  at the surface. The initial data used for our investigation is based on a composite of data collected during the recent Rain in Cumulus over the Ocean (RICO) field study (Raubert et al. 2007). Nearly identical initial data is used in the intercomparison study by the GCSS<sup>2</sup> boundary layer working group, the only difference being that

the GCSS initial data interpolates the initial profile of  $r_i$  to a drier (2.4 versus 4.4  $\text{g kg}^{-1}$ ) value at 3260 m. Because it corresponds to the GCSS intercomparison case, sensitivities to numerical aspects of the solution are explored using this drier initial data, as discussed in Section 2.d below.

Surface fluxes are calculated based on the fixed surface properties and those at the first grid level using a bulk aerodynamic formulation with fixed exchange coefficients of  $C_h = 0.001094$ ,  $C_r = 0.001133$ , and  $C_m = 0.001229$  for heat, moisture and momentum respectively. Large-scale thermodynamic tendencies associated with advection and radiation are imposed to provide balanced initial data in the free atmosphere, such that

$$\left(\frac{\partial \chi}{\partial t}\right)_{LS} = -W \frac{\partial \chi}{\partial z} + Q_\chi, \quad (19)$$

where here  $\chi$  denotes either  $\theta_i$  or  $r_i$ , and  $W = -0.005 z/z_w$  with  $z_w = 2260 \text{ m}$ . The autonomous source terms  $Q_\chi$  are specified as

$$Q_{\theta_i} = -2.5 \text{ K d}^{-1}, \quad (20)$$

$$Q_{r_i} = -1 + 1.3456 \frac{\min(z, z_r)}{z_r} \text{ g kg d}^{-1}, \quad (21)$$

with  $z_r = 2980 \text{ m}$ .

*c. Simulation methodology*

Unless otherwise noted, all simulations are performed over a domain that is 5 km deep and 19.2 km on a side. The horizontal discretization is 100 m and the vertical discretization is 40 m. The model timestep is variable, chosen to maintain the maximum Courant number within the domain between 0.65 and 0.85. The base droplet concentrations were fixed at  $N_c = 70 \text{ m g}^{-1}$ , in correspondence with the average conditions as observed during RICO. Each simulation was run for 24 simulated hours, profile statistics are presented as an average over the last five hours of the simulations, time-series statistics are presented in tables and averaged over the last four hours of the simulations.

The time-series data includes the cloud and rain water paths, defined as

$$\mathcal{L} = \int_0^\infty r_c \rho dz \quad \text{and} \quad \mathcal{R} = \int_0^\infty r_r \rho dz.$$

2 Global Energy and Water Experiment Cloud Systems Studies

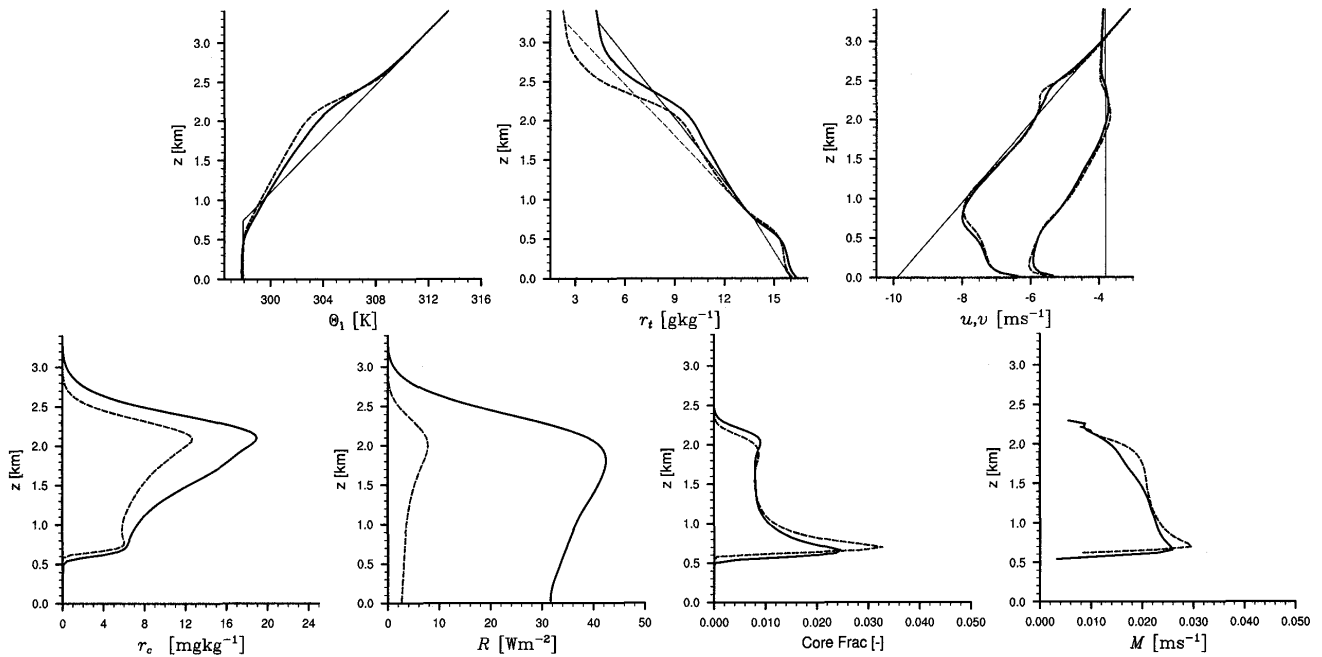


Fig. 1. Mean profiles of control (black) and drier GCSS case (gray) and initial conditions (thin lines upper panels). Shown in upper panels from left to right are liquid water potential temperature, total-water mixing ratio and zonal/meridional winds. On lower panels from right to left are domain averaged cloud water, precipitation flux, conditionally averaged cloud core fraction and core mass flux.

Two types of cloud-cover statistics are presented. The first, denoted  $C$ , is the number of cloudy columns at a given time. The second is the cloud core fraction and varies with height. Following previous cumulus studies (cf., Siebesma et al. 2003) the cloud core denotes a conditional average over cloudy buoyant air. The depth of the convective layer is denoted  $z_i$  which is defined as the average height of the maximum  $\theta_l$  gradient at a particular time. This quantity is computed in each column and averaged over the domain. Two measures of the rain rate are presented. The first,  $R$ , measures the rain rate at the surface the second,  $R_{mx}$  measures the maximum value of the time-averaged rain profile. Because the averaging periods of the profile statistics and the tabulated data are slightly different, tabulated rain-rates are not identical to those derived from the profiles shown as figures.  $N_R$  denotes  $n_r$ , conditionally averaged over grid-cells where  $r_r > 1 \text{ mg kg}^{-1}$ . Unless otherwise stated statistics are accumulated every 30s of simulation time and then averaged over the last four hours of the simulation.

*d. Baseline behavior*

Context for our exploration of microphysical effects is provided in this sub-section where we

detail basic features of the simulated flow as well as its sensitivity to changes in the initial data or the structure of the underlying grid upon which our equations are solved.

The initial data supports the emergence of a shallow layer of cumulus clouds after about 2 hrs of simulated time. Thereafter the cloud layer progressively deepens and moistens, reaching a depth of about 2400 m after 24 hrs, with cloud base remaining near 600 m, and cloud fractions steady at about 15%, and relatively constant surface fluxes, through the course of the simulation. The vertical structure and the temporal evolution of the simulations is shown in Figs. 1 and 2 respectively. Precipitation is intermittent, indicating that precipitation events are not well sampled on the scale of the domain, but tend to increase in intensity with the development and deepening of the cloud layer. Domain averaged precipitation rates over the last four hours average about  $30 \text{ W m}^{-2}$ , or a little over  $1 \text{ mm d}^{-1}$ , similar to what was inferred based on an analysis of radar data during RICO.

The flow evolution exhibits a marked sensitivity to the initial humidity data. Simulations developing from an initially drier mean state (gray lines in Figs. 1 and 2), exhibit significant differences in the thermodynamic structure of the cloud layer

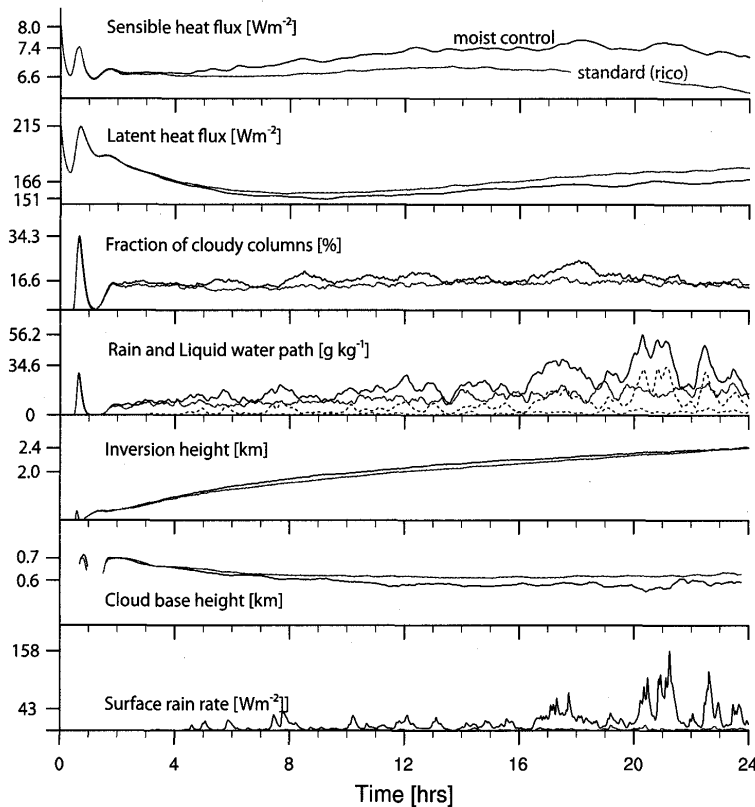


Fig. 2. Time-series showing evolution of the control case and a simulation using the drier (GCSS) initial data. In this figure the liquid water path refers to the sum of the cloud and rain-water paths. The rain-water path is given by the dashed lines in the fourth panel.

and precipitation, although the energetics of the clouds themselves (as measured by their mass flux and core fraction) remain relatively unchanged. Rain production from the drier-layer is relatively anemic. Differences in the cloud water profiles appears to be more a consequence and less a cause of differences in the rate of precipitation: In non-precipitating simulations (not shown) using both sets of initial data, the cloud water between the two simulations is more similar, except that the moist initial data supports a deeper cloud layer and hence more cloud-top liquid water. A difference that is diminished when precipitation is allowed to form. The development of precipitation in the simulation with moister initial data is also associated with a much larger fraction of the total condensate path being carried by the rain water.

The development of precipitation was also found to be sensitive to details of the numerical implementation. For instance, the simulations starting from relatively dry initial data precipitated more effectively as the grid spacing was coarsened, or the grid as a whole was enlarged. This behavior is evident in Fig. 3 and Table 2 which show pronounced

increases in precipitation as the mesh is coarsened from its default spacing. Less pronounced changes as the mesh is refined from its default size motivate our choice of mesh.

There is a tendency is to think that more variance within a cloud will increase the chances that sufficient cloud water develops to initial precipitation (e.g., Chen and Cotton 1987; Larson et al. 2001). But experience with deep convection has also shown that poorly resolved simulations lead to more overturning on larger scales, which leads to less dilute overturning plumes (William R. Cotton, personal communication, 2008). This latter experience is in accord with our findings. As the resolution becomes coarser than the base resolution the clouds become progressively less dilute (the cloud-core liquid water lapse rate increases by more than 50% as  $\Delta x$  increases from 100 to 400 m) thereby supporting the development of more precipitation. For grids finer than the control resolution differences in the precipitation profiles are relatively more modest (the cloud-core liquid water profiles are also quite similar), suggesting that the base resolution may be adequate to begin seeing how

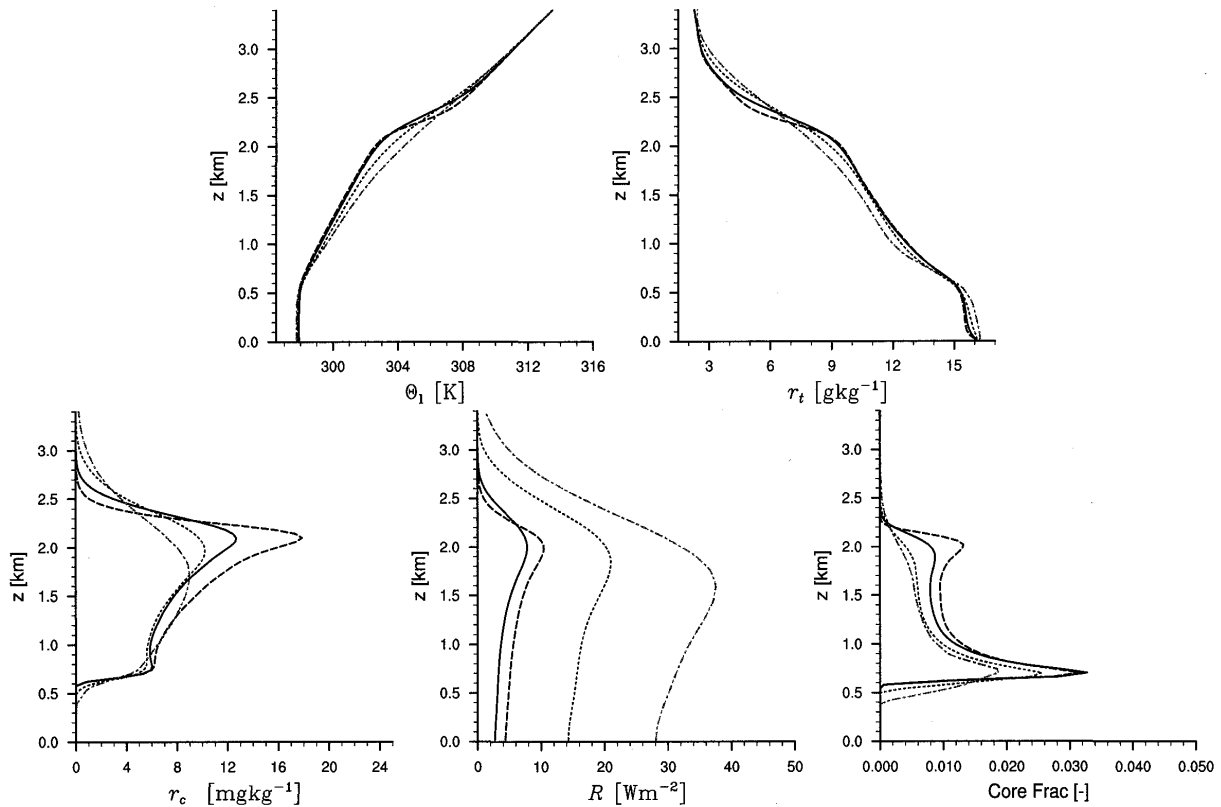


Fig. 3. Mean profiles at four different resolutions for drier (GCSS) initial data:  $\Delta x = 2.5\Delta z = 50$  m (solid), 100 m (control, dashed), 200 m (dotted, 400 m dash-dot). Upper panels show  $\theta_1$  and  $r_r$ , lower panels show from left to right,  $r_c$ , rain-rate and core cloud fraction.

Table 2. Sensitivity to resolution for  $N_c = 70 \text{ mg}^{-1}$  given drier (GCSS) initial data. Here  $\Delta z = \Delta x/2.5$  Other columns are cloud-water path [ $\text{g m}^{-2}$ ], rain-water path [ $\text{g m}^{-2}$ ], fraction of columns with cloud, inversion height [m], surface rain rate [ $\text{W m}^{-2}$ ], maximum time and horizontally averaged rain rate in layer [ $\text{W m}^{-2}$ ], and rain-drop concentrations [ $\text{dm}^{-3}$ ] averaged over raining regions. <sup>1</sup> Denotes a different random seed.

$N_x$	$\Delta x$	$\mathcal{L}$	$\mathcal{R}$	$C$	$z_i$	$R$	$R_{mx}$	$N_R$
384	50	16.8	3.8	0.19	2248	5.9	12.3	12.8
512	100	15.0	4.8	0.13	2349	6.9	14.2	15.5
256	100	15.0	2.9	0.13	2346	4.9	12.2	15.4
192	100	14.2	3.0	0.13	2346	3.2	9.2	14.5
128	100	14.4	2.4	0.13	2335	2.4	7.6	13.6
128	100 <sup>1</sup>	13.9	2.5	0.13	2334	2.5	8.4	13.7
128	200	11.5	7.5	0.08	2390	16.1	24.8	17.1
128	400	8.6	12.3	0.05	2442	35.6	44.3	12.4

changes in the microphysical representation affects the simulation statistics. But even so, at finer resolution a marked sensitivity of the inversion structure, and cloud-top cloud amount, remains. These results suggest that numerical diffusion in the inversion is playing an undesirably large role in setting the structure of the cloud at that level, and suggesting that even at grid spacings of  $\Delta x =$

100 m and  $\Delta z = 40$  m our representation of shallow clouds may at best be marginal.

Finally, we briefly explore the statistical robustness of the case starting from drier initial data, by comparing two simulations initialized with different random seeds. The differences between these simulations are much smaller than the other differences we have, or will discuss. And although all

Table 3. As in Table 2 but as a function of droplet numbers with both KK and SB microphysics for the control (moist) case.

$N_c$	Microphysics	$\mathcal{L}$	$\mathcal{R}$	$C$	$z_i$	$R$	$R_{mx}$	$N_R$
35	SB	13.0	16.8	0.13	2183	36.5	53.1	25.9
70		17.4	17.3	0.14	2368	42.3	50.1	16.9
105		20.0	6.5	0.17	2477	11.6	19.1	10.4
140		19.8	3.9	0.18	2494	8.1	11.4	7.5
35	KK	14.7	30.5	0.11	2271	37.5	86.7	16.9
70		20.3	3.1	0.18	2506	2.3	9.0	5.0
105		20.5	1.4	0.18	2527	1.8	4.4	3.4
140		20.9	0.4	0.19	2508	0.3	1.1	3.0

of our subsequent analysis is based on simulations developing from the moister initial data, we have no reason to expect that they would exhibit sensitivities to the numerical mesh, and random seed, incommensurate to what was shown based on simulations developing from drier initial data.

### 3. A posteriori analysis (the simulations)

For the base case, simulations with KK produce precipitation less efficiently than simulations with SB microphysics. Both schemes produce a marked sensitivity of the rain rate to the number concentration, although the number concentration at which this occurs varies depending on the scheme. Table 3 summarizes these findings in terms of pertinent integrals from the simulations. Those with KK have a marked transition in rain rate between what one might call clean, and very clean, maritime conditions—corresponding to droplet concentrations between 35 and 70  $\text{mg}^{-1}$ . For SB this transition occurs more gradually and is centered at more modest droplet concentrations, between 70 and 105  $\text{mg}^{-1}$ . Simulations with both models suggest that cloud fraction and liquid water path decrease with increasing precipitation, although again such changes appear to be more gradual in the simulations using SB. Finally, larger values of  $R_{mx}/R$  in the KK relative to the SB simulations suggests the former are more effective in reducing precipitation through evaporation.

In all cases precipitation is effective in arresting the growth of the cloud layer, as  $z_i$  decreases with increasing  $R$  in most cases. While such a result was anticipated based on theoretical arguments (Stevens 2007) it complicates simple relationships between microphysical processes and macrophysical outcomes. Processes which can suppress rain,

may lead to deeper clouds that then develop more rain. One way to control for this effect is to be mindful of the depth of the cloud layer (as indicated by  $z_i$ ) when comparing the simulations. So for instance, as  $N_c$  is further reduced from 70 to 35  $\text{mg}^{-1}$  in the simulations with SB, precipitation does not increase markedly (it actually decreases at the surface). However, the cloud layer remains shallower. An analysis of the time-series of the surface rain rate (Fig. 4) supports the idea that the efficient production of rain retards the growth of the cloud layer in the early stages of the simulation, leading to a shallower cloud layer and less rain overall. We take for granted that deeper clouds—*ceteris paribus*—rain more readily.

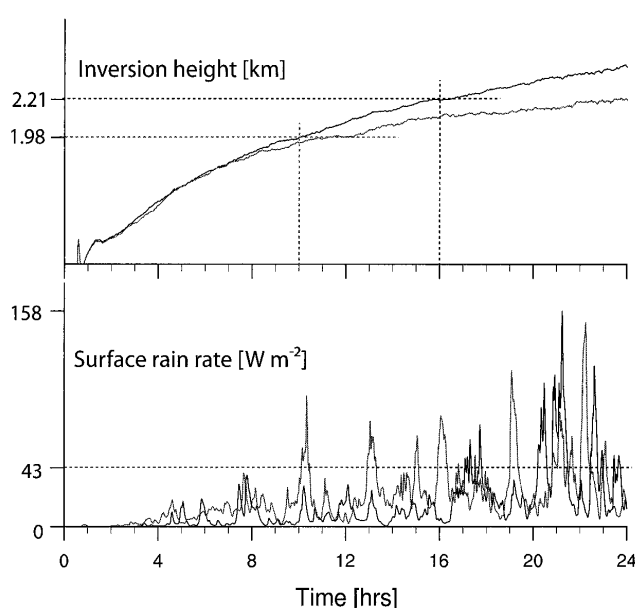


Fig. 4. Time-series showing evolution of inversion height and surface rain rate for  $N_c = 70$  (black) and 30 (gray)  $\text{mg}^{-1}$ .

In Table 4 we present statistics for a large number of additional simulations, wherein we systematically vary components or parameters of the microphysical models used in the simulations. Our motivation in doing so, and a goal of this study, is to better understand in which way and to what degree the overall bulk statistics of a simulation are sensitive to the various components or parameters, and whether or not such sensitivities are consistent with an *a priori* analysis of the schemes. The main points in the table can be summarized as follows:

1. Pronounced sensitivities to the formulation of the terminal velocity (as controlled by the choice of  $\mu$  in the formulation of sedimentation, simulations S01-S05, see also Fig. 5) become evident as  $\mu$  approaches zero, but differences among simulations with  $\mu$  given by Eq. 6 or set to some constant value significantly greater than zero, are relatively modest. Narrower distributions (larger values of  $\mu$ ) tend to produce more rain at the surface.
2. SB auto-conversion produces rain more efficiently than KK (compare S01, S03, S09 and S10). To the extent auto-conversion is the only processes limiting the surface rain rate Table 3 suggests that  $N_c$  must be reduced from 70 to 35  $\text{mg}^{-1}$  before KK produces rain as efficiently as SB.
3. Maximum rain-rates vary more gradually with  $N_c$  for SB, than they do for KK. This is evident in relationship between  $R_{mx}$  and  $N_c$  in Table 3), particularly at high number concentrations.

4. The inclusion of self-collection in SB plays an important role in reducing the number of rain drops, so that in the absence of other effects self-collection leads to larger rain drops which are less susceptible to evaporation (compare the difference between  $R_{mx}$  and  $R$ , which we attribute to evaporation, in S06 and S01). The results suggest that aside from differences in

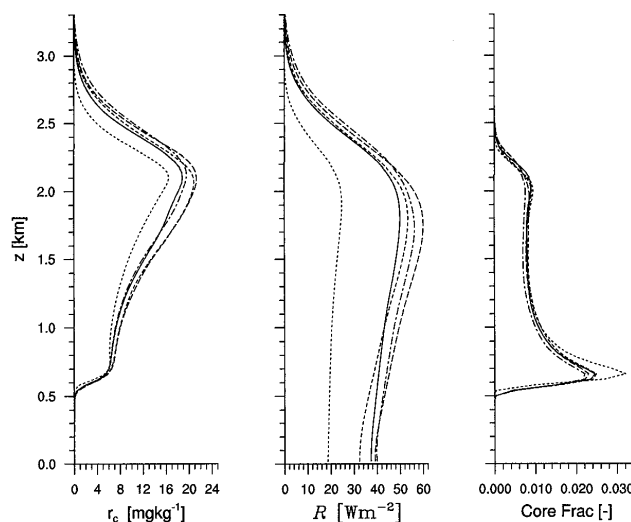


Fig. 5. Profile of cloud water, rain rate and cloud-core fraction for simulations as a function of the representation of the terminal velocity of microphysical moments: parameterized  $\mu$  (solid)  $\mu = 0$  (dotted),  $\mu = 5$  (short dash),  $\mu = 10$  (long dash), KK (dash-dot).

Table 4. Tabulation following Table 2, with simulations named for purposes of referencing within the text. The parenthetical triplets associated with the microphysical description refer to the processes of auto-conversion, accretion, and sedimentation. Hence (SB, KK, SB) as appears in the comment for 09 indicates an SB treatment of auto-conversion and sedimentation, but a KK treatment of accretion. Unless otherwise indicated the SB representation of accretion incorporates self-collection, but not break-up.

Name	Microphysics	$\mathcal{L}$	$\mathcal{R}$	$C$	$z_i$	$R$	$R_{mx}$	$N_R$
S01	SB	17.4	17.3	0.14	2368	42.3	50.1	16.9
S02	SB- $\mu = 0$	16.6	6.8	0.16	2357	18.0	24.9	14.9
S03	SB- $\mu = 5$	18.9	19.4	0.15	2368	31.0	53.6	18.4
S04	SB- $\mu = 10$	18.3	22.7	0.15	2401	42.4	60.2	16.7
S05	(SB, SB, KK)	16.8	20.8	0.13	2431	40.3	56.4	16.8
S06	SB (no SC)	22.8	38.1	0.17	2452	27.6	85.9	64.0
S07	(SB, KK, SB)	20.4	20.3	0.15	2273	42.9	99.3	57.0
S08	KK	20.3	3.1	0.18	2506	2.3	9.0	5.0
S09	(SB, KK, KK)	22.4	55.6	0.16	2348	18.1	95.5	58.3
S10	(KK, SB, SB)	18.9	1.6	0.18	2505	2.7	7.0	3.9
S11	S03 with Breakup	16.2	19.6	0.13	2335	36.5	53.0	16.7
S12	S11 with Ventilation	14.7	15.6	0.11	2336	23.0	62.9	21.6

auto-conversion, the largest difference when switching between the SB and KK microphysical representations is probably due to the lack of self-collection.

5. The larger surface rain-rates, reduced rain-water path, and diminished rain-drop number mixing ratios in S07, relative to S06, are all consistent with a more aggressive representation of accretion by KK.
6. Breakup (which includes drop rebound effects) and ventilation effects are not insignificant (S11 and S12). While such processes appear to play a more minor role in setting the character of the simulations than does, for instance, one's choice of auto-conversion, they merit consideration for simulations of shallow convection.

Given a core fraction of one to two percent, and domain averaged rain rates of some tens of watts per square meter, one might expect the rain formation to be associated with the development of pronounced but isolated rain events. This is consistent

with the episodic character of the surface rain-rate time-series, the importance of self collection (point 3 above), and the difference between the  $\mu = 0$  and the parameterized  $\mu$  simulations (point 1 above). Flow analysis focusing on the spatio-temporal evolution of a typical precipitation event confirms this speculation—as illustrated, for instance, by the time-evolution of radar reflectivity in the bottom panels of Fig. 6.

Our flow analysis, which is encapsulated by the example in Fig. 6, further introduces the idea that the convective structures which developed, and produced precipitation, were relatively simple. Convective thermals developed in the sub-cloud layer, formed incipient clouds that, if they became sufficiently deep, developed precipitation at their leading edge, which falls to the surface in a rain-shaft.

The early period of cloud development is not shown, but typical. Seven minutes prior to the first snapshot the cloud evinces a well defined base near 500 m and updraft, and a cloud top at 1400 m with

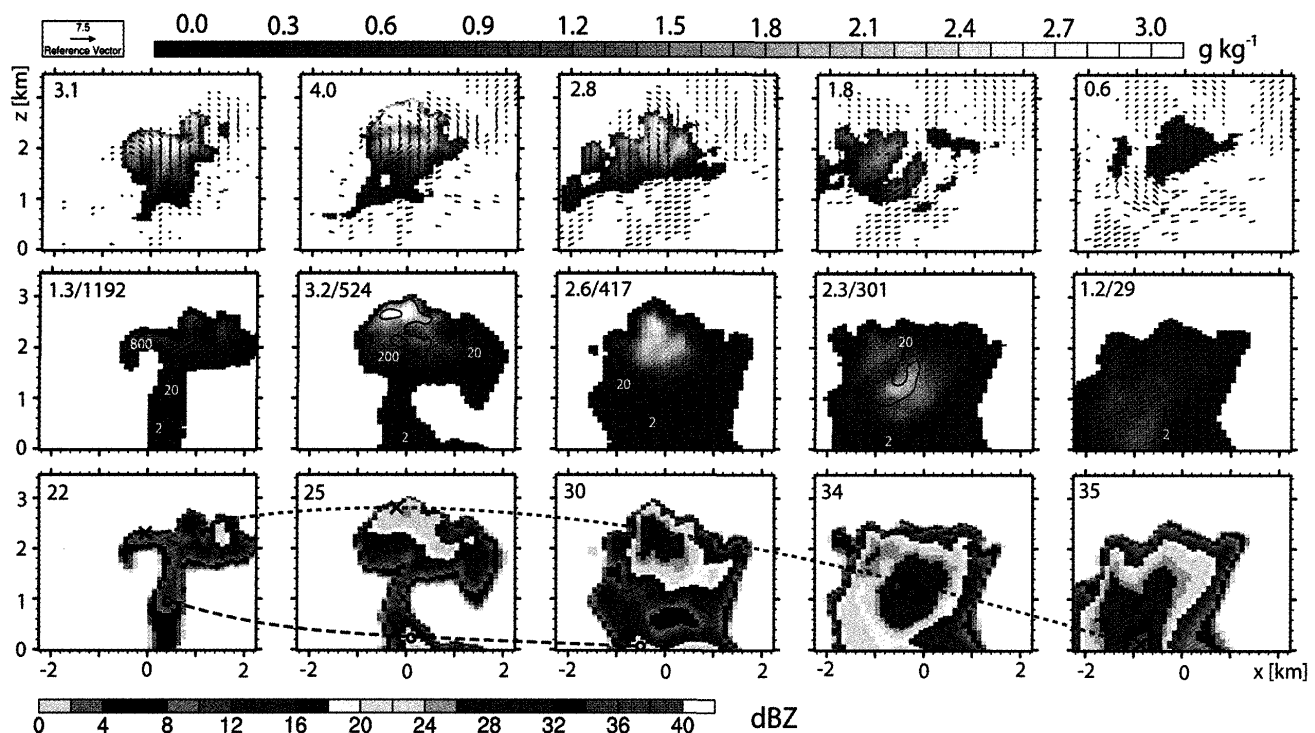


Fig. 6. Time slices at 210 s (3.5 min) intervals showing the evolution of a vigorous cloud in the  $x$ - $z$  plane. The flow is taken from a simulation configured as S11 but initialized from the 16 h restart file of S10. The analysis is about 90 min after the restart. Each slice is only a small portion of the total domain. Shown are cloud water and  $u, w$  velocities in upper panels; rain water and rain number mixing ratios (lines) in middle panels; radar reflectivity for  $\mu = 5$  in lower panels. Velocity vectors in upper panel are placed every other point in  $x$  and every third point in  $z$  direction in regions where  $|w| > 0.5 \text{ m s}^{-1}$ . Number concentrations are in units of  $\text{g}^{-1}$  (roughly corresponding to concentrations of per liter.)

no rain. 3.5 min later (still 3.5 min before the first panel in Fig. 6), the updraft and cloud base are still well defined, cloud top is just below 2 km and still no rain has developed. The first snapshot coincides with the first sign of precipitation development. The feature we wish to focus on is marked by the cross in the radar-reflectivity panel, corresponding to the leading edge of the thermal (at about 2.3 km) where cloud water is greatest, and the production of large-amounts of small rain drops (middle panel) is evident. At this time the base of the cloud is already eroding, i.e., the cloud is decaying well in advance of the development of significant precipitation. By the time of the next snapshot the cloud top has risen by nearly 700 m (an advance of about  $3 \text{ m s}^{-1}$ ), accompanied by the development of significant amounts of rain water, and the intensification of the maximum echo from about 10 dBz to 25 dBz, cloud base has further eroded, but the echo tracks the region of maximum cloud water. Thereafter the rain-drops continue to get larger (as evidenced by the depletion of drop number concentrations), the echo intensifies to 30 dBz and begins to descend through the decaying thermal. An organized downdraft also emerges through the center of the thermal. The last two frames show the continued descent of the maximum radar echo, and its further intensification, consistent with self-collection being active. Upon reaching the surface 14 min after the first snapshot it is descending at a rate of nearly  $7 \text{ m s}^{-1}$  and has intensified to a magnitude of about 35 dBz. Meanwhile the condensate associated with the original cloud lingers aloft, energetically disconnected from the surface.

The picture is complicated by the presence of an earlier rainshaft (marked by the open circle near cloud base in the first radar-reflectivity snapshot). While the tendency of precipitation to develop in the vicinity of previous precipitation appears to be common in the simulation, at least in this case however, the development of rain in the primary echo is unlikely to have been influenced by the earlier event. This argument follows from the appearance of large-concentration of rain-drops produced in situ as shown in the middle panel of the first snapshot. Apart from providing a basis for more quantitative comparisons with data, for instance from RICO, this analysis suggests that the simulations develop rain in relatively simple ways.

#### 4. A priori analysis (component processes)

The apparent simplicity of rain development in the simulated clouds motivates an analysis of the component microphysical models in simplified dynamic environments. Our goal in this section is to create a framework that allows us to understand the macroscopic outcomes of the microphysical changes as presented above. We discuss sedimentation and component kinetic processes in turn. The effects of thermodynamic processes, namely evaporation, are not explored at this time.

##### a. Sedimentation

One known limitation of a two-moment representation of cloud microphysics is that the shape of the drop distribution is not invariant under sedimentation. Big drops fall fast and small drops linger, which narrows the distribution in mass space while broadening it in physical space. As shown by Wacker and Seifert (2001), failure to account for such effects can lead to unphysical behavior, such as the development of shocks. To mitigate such effects Milbrandt and Yau (2005) proposed parameterizing the shape parameter in terms of the mean diameter. Their idea motivates the parameterization (6) which narrows the distribution as drops becomes larger.

Differences in  $w_v$  as a function of ones choice of  $\mu$ , or underlying fall-speed model, are shown with the help of Fig. 7. Differences in  $w_v$  are most evident in what we call the sorting ratio:  $w_r/w_n$ . However, differences of tens of percent in the sorting ratio translate into relatively small differences in the macroscopic evolution of the simulations. It is only for the limiting (and, we note, not necessarily uncommon) assumption of  $\mu = 0$  that significant differences among the simulation emerge. Although the emergence of this sensitivity would have been difficult to predict based on the behavior of Fig. 7, it does emerge from an analysis of solutions to the one-dimensional sedimentation equation, which for a constant density fluid is,

$$\frac{\partial \psi}{\partial t} = -\frac{\partial}{\partial z}(w_v \psi). \quad (22)$$

Following Wacker and Seifert (2001) we solve for an initial pulse of rain-water distributed uniformly with height over a 500 m layer and initially distributed exponentially as a function of mass (cf., Marshall and Palmer 1948). This choice of initial data allows

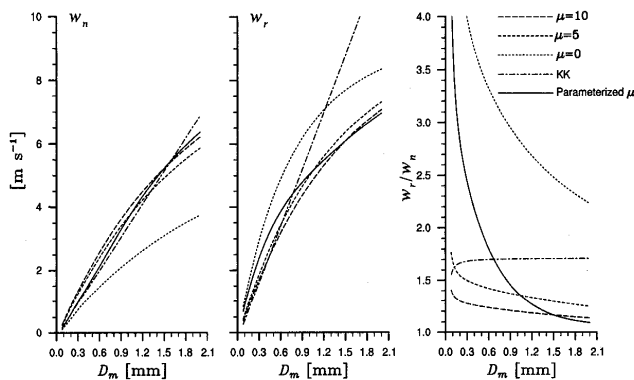


Fig. 7. Terminal velocities for selected moments of the distribution, and their ratio, for different fall-speed relations and shape parameters.

one to integrate (22) analytically to yield  $r_c(z,t)$ . Otherwise, the initial conditions are loosely based on the simulations. Solutions which maintain  $\mu$  at its initial value of zero when determining  $w_v$  diverge most from the analytic solutions. Because of the size sorting, the distribution too rapidly narrows in diameter space, and hence unrealistically broadens in physical space. As a result the great mass of rain-water falls much less rapidly to the surface than would be predicted by a distribution which maintained  $\mu$  fixed at zero. Although assuming  $\mu > 0$  misrepresents the distribution at the initial time, it provides a more (if not completely) satisfactory representation of the evolution of  $n_r$  and  $r_r$ . Interestingly, the fact that the cases with  $\mu > 0$  are more similar to one another than they are to the analytic solution, suggests that simulations which were capable of more realistically representing the sedimentation process, could still depart significantly from the consensus result in Fig. 5.

Based on the above analysis, why does the simulation with  $\mu = 0$  develop less rain overall? One interpretation is that in this limit the sedimentation scheme moves mass too rapidly to the surface. So doing desiccates the leading edge of the cloud thus hindering the development of more than an initial pulse of rain.

#### b. Auto-conversion and accretion

Why do the simulations with SB auto-conversion develop rain more efficiently than those with KK, and why do simulations with KK shut down the warm-rain production more distinctly as cloud-droplet number concentrations increase?

The strength of auto-conversion component of

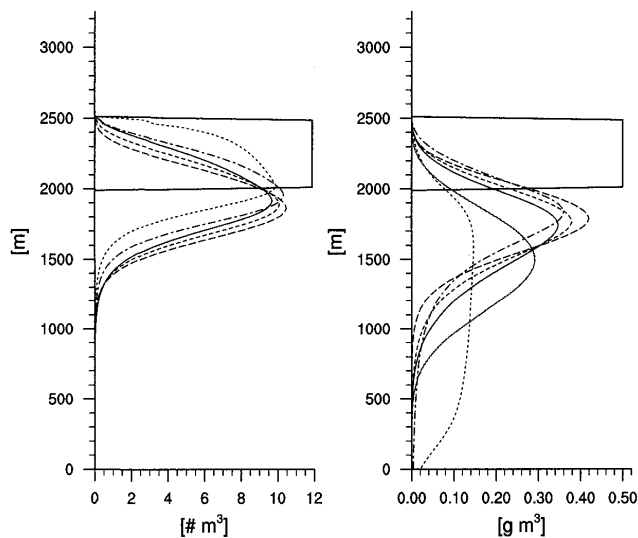


Fig. 8. Evolution of a pulse of rain after 250s due only to sedimentation affects. Line labeling as in Fig. 7, except for the solid gray lines which show the initial conditions in dark gray as a square pulse, and the analytic solution for  $r_r$  in light gray. Drop number,  $n_r$ , (left panel) and mass mixing ratio (right panel).

SB and KK (the first term on the rhs in (8) and (15)) is shown as a function of  $r_c$  in Fig. 9a. At first glance this behavior might appear to contradict the findings from the LES, but such a comparison fails to account for the dependence of the SB auto-conversion on  $\phi_{cc}$ , and so in panel (a) we show the rate of the SB auto-conversion process in the absence of spectral ripening effects, i.e.,  $\phi_{cc} = 1$ , while panel (b) shows the value of  $\phi_{cc}$  required for auto-conversion to be commensurate between the two schemes. Panel (c) plots  $\phi_{cc}$  over the domain of its argument,  $\varepsilon$ . From the underlying equations it is apparent that without the spectral ripening the SB scheme is more efficient at converting cloud droplets to rain drops for  $r_c > (a_{hk}/a_{sb})^{9/19} N_c^{1/19} \approx 2.5 \text{ g kg}^{-1}$ . As is evident in Fig. 6 such large values of  $r_c$  are apparent locally in the simulated clouds, although on average cloud-water mixing ratios may be a factor of two or more smaller.

To more quantitatively explore the behavior of the auto-conversion and accretion parameterizations we analyze the simple parcel model:

$$\frac{dr_c}{dt} = \frac{1}{\tau_c} - \mathcal{K}_r. \quad (23)$$

$\tau_c^{-1}$  is the condensation timescale,  $\mathcal{K}_r$  is given by

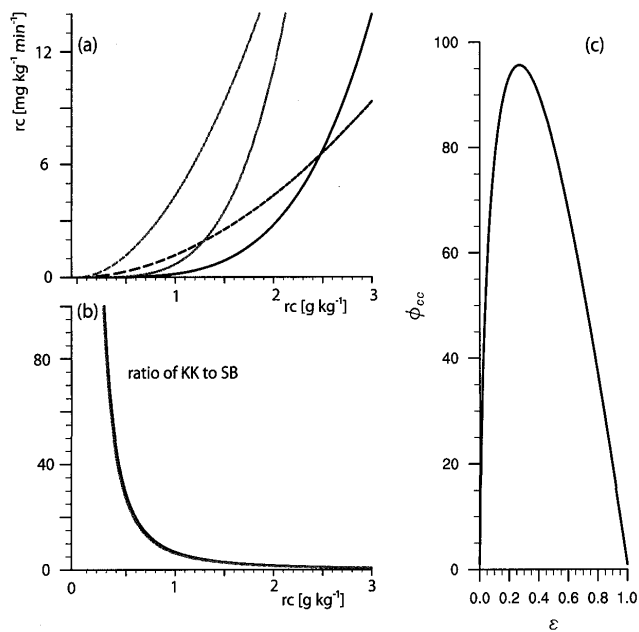


Fig. 9. Differing efficiency of SB with  $\phi = 1$  (solid) and KK (dashed) auto-conversion schemes for cloud-droplet concentrations of  $70 \text{ mg}^{-1}$  (black) and  $30 \text{ mg}^{-1}$  gray (panel a). Ratio of KK auto conversion rate to that of SB for cloud-droplet concentrations of  $70 \text{ mg}^{-1}$  (black) and  $30 \text{ mg}^{-1}$  gray (panel b). Dependence of  $\phi$  on progress variable  $\varepsilon$  (panel c).

either the microphysical model (8) or (15) and sedimentation is neglected. Equation (23) is the complement of the rain shaft model given by (22). Physically (23) can be interpreted as describing the evolution of the cloud water for ascending parcels, in which case  $\tau_c^{-1} = w\Gamma_l$  where  $\Gamma_l$  is the liquid-water lapse rate and  $w$  is the updraft velocity. From this perspective mixing can be parameterized by fixing  $\Gamma_l$  less than its adiabatic value. Mathematically (23), with its associated microphysical model, constitutes an initial value problem consisting of two coupled first order differential equations. We integrate them numerically with  $r_c(t = 0) = r_r(t = 0) = 0 \text{ g kg}^{-1}$  for the initial conditions, and explore their behavior as a function of the microphysical model and the parameters,  $\tau_c$  and  $N_c$ . Although nothing prevents the condensation rate from varying in time, here we evaluate the model for  $\tau_c$  fixed.

Results from integrations of (23) demonstrate that the  $\phi_{cc}$  term is decisive, as it leads to more efficient cloud to rain water production in the SB scheme even at values of  $r_c$  well below  $2.5 \text{ g kg}^{-1}$ . A sample integration is plotted in Fig. 10 for the

case of  $\tau_c$ ,  $0.588 \times 10^6 \text{ s}$  and  $N_c = 70 \times 10^6 \text{ kg}^{-1}$ . The condensation timescale was chosen to match that of conditionally averaged cloudy cores in the simulations, for which we find  $\Gamma_l \approx 0.85 \text{ g kg}^{-1} \text{ km}^{-1}$  and  $w \approx 2 \text{ m s}^{-1}$ . Solutions to (23) show cloud water increases with time at the prescribed rate, until the parameterized collision-coalescence process becomes efficient at converting cloud water to rain. We denote, by  $t_*$  the time at which  $dr_c/dt = 0$ . Loosely thinking,  $t_*$  measures the onset time for precipitation development; thereafter the water is very efficiently converted to rain. From the figure this occurs at about  $r_c = 1.35$  and  $1.55 \text{ g kg}^{-1}$  for SB and KK respectively. Given the cloud-core liquid-water lapse rates, and a cloud base height of 500 m, this cloud water concentrations correspond to clouds of depths near 2.1 and 2.3 km respectively.

Figure 10 also shows that while the small differences in the representation of accretion between the two schemes do not appreciably affect  $t_*$ . They do control the long-time equilibrium cloud water in the model, and its approach to this equilibrium (i.e., the rate at which  $r_c$  is depleted for  $t > t_*$ ). A more active accretion process in KK significantly accelerates the conversion of cloud-water to rain water in the period just after  $t_*$ . This behavior is consistent with the simulations, where we recall those that differed only in the representation of accretion (S06 and S07) precipitated more efficiently with KK accretion.

One can gain insight into  $t_*$ , and what aspects of the schemes are responsible for determining it, by noting that at this time

$$\mathcal{K}_r|_{t_*} = \tau_c^{-1}, \tag{24}$$

where the lhs is given by the microphysical model, e.g., (8) or (15). From the definition of  $\varepsilon$ , in (12), we note that  $r_c = (1 - \varepsilon)r_l$  and  $r_r = \varepsilon r_l$  where  $r_l = r_r + r_c$ . Given these relations and recognizing that  $r_l = t/\tau_c$  it is straight forward to derive implicit equations for  $t_*$  from (24) in terms of  $\varepsilon$ , namely

$$a_{sb} \left[ \frac{(1 - \varepsilon)t_*}{\tau_c N_c^{1/2}} \right]^4 \phi_{cc}(\varepsilon) + b_{sb} \left( \frac{t_*}{\tau_c} \right)^2 (1 - \varepsilon)\varepsilon \phi_{cc}(\varepsilon) - \frac{1}{\tau_c} = 0, \tag{25}$$

and

$$a_{kk} \left[ \frac{(1 - \varepsilon)t_*}{\tau_c N_c} \right]^{17/9} + b_{kk} \left[ \left( \frac{t_*}{\tau_c} \right)^2 (1 - \varepsilon)\varepsilon \right]^{1.15} - \frac{1}{\tau_c} = 0, \tag{26}$$

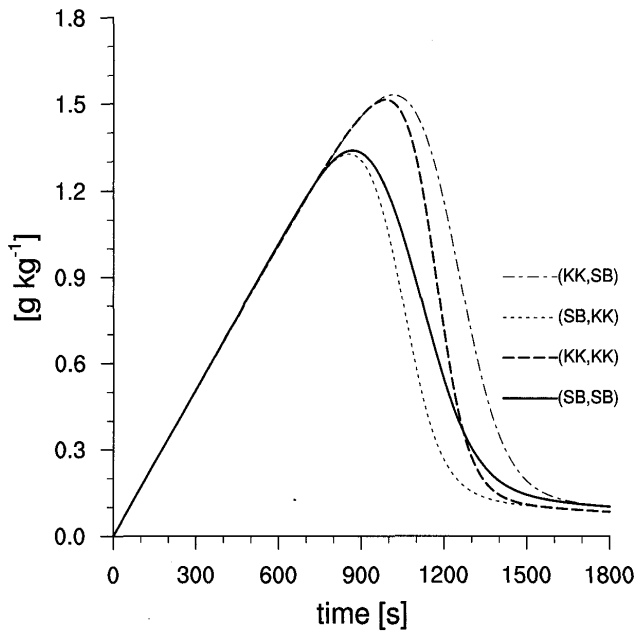


Fig. 10. Time evolution of  $r_c$  for different microphysical choices as indicated by the pairs, i.e., (XX,YY) denotes auto-conversion by scheme XX and accretion by scheme YY. Solutions are for  $\tau_c = 5.88$  Ms and  $N_c = 70 \text{ mg}^{-1}$ .

for the microphysical models (8) and (15) respectively. Equation (25) can be written explicitly in terms of  $\varepsilon$ ,

$$t_*^{(sb)} = \left[ \beta_{sb} + \sqrt{\beta_{sb}^2 + \frac{(t_0^{(sb)})^4}{(1-\varepsilon)^4 \phi_{cc}}} \right]^{1/2} \quad \text{where} \quad (27)$$

$$\beta_{sb} = N_c^2 \frac{b_{sb}}{2a_{sb}} \frac{\varepsilon \phi_{cr}}{(1-\varepsilon)^3 \phi_{cc}}$$

and

$$t_0^{(sb)} = N_c^{1/2} \tau_c^{3/4} (a_{sb})^{-1/4}, \quad \text{where} \quad t_0 \equiv \lim_{\varepsilon \rightarrow 0} t_* \quad (28)$$

Likewise,

$$t_0^{(kk)} = N_c \tau_c^{8/17} a_{kk}^{-9/17} \quad (29)$$

Equations (28) and (29) suggest that  $t_*$  should increase with  $\tau_c$  and  $N_c$ , thereby agreeing qualitatively, but quantitatively the scaling is carried by different exponents. In the SB model  $t_0$  depends less strongly on  $N_c$  and more strongly on  $\tau_c$  than it does for the KK model, which depending on the size of the constants, suggests that KK will produce precipitation relatively more efficiently in the

“continental” limit (large  $N_c$ ). These inferences are borne out in Fig. 11 where  $t_*$  is evaluated numerically and plotted as a function of  $\tau_c$  and  $N_c$ . The figures show that  $t_0$  does a good job of predicting how  $t_*$  depends on  $\tau_c$  but poorly represents the dependence of  $t_*$  on  $N_c$ . This is especially true for KK, where  $t_0$  and  $t_*$  only appear to be related in the limit of vanishing  $N_c$ .

The degree to which  $t_*$  and  $t_0$  behave differently can be taken as a measure of the relative efficacy of accretion, even for small  $\varepsilon$ . For our simple model the presence of accretion weakens the dependence of  $t_*$  on  $N_c$ , with the more aggressive KK representation of accretion acting even more strongly in this direction. The dependence of  $t_*$  on  $N_c$  appears to be controlled by the representation of accretion at large  $N_c$  as evident for instance in panel (b) of Fig. 11 where calculations are performed with KK auto-conversion and SB accretion, and *vice versa*. The importance of accretion to  $t_*^{(kk)}$  is not surprising, from (29) it is apparent that auto conversion alone becomes effective at depleting the production of water through saturated ascent only when  $r_c = N_c (\tau_c a_{kk})^{-17/9}$ . For the parameters used here, this only occurs at extraordinarily high ( $r_c \approx 10 \text{ g kg}^{-1}$ ) liquid-water mixing ratios. Hence the degree to which  $t_0$  misrepresents the dependency of  $t_*$  on  $N_c$  partially reflects the weakness of the exponents in the cloud water dependency of auto-conversion. Wood (2005) argues, based on an analysis of aircraft data of stratocumulus, that auto-conversion should be  $\propto r_c^3$  which is stronger than KK, but weaker than SB (for which auto-conversion is  $\propto r_c^4$ ). Whether his analysis generalizes to precipitating cumulus, and the larger critical diameters we use here ( $D_* = 80$  versus  $40 \mu\text{m}$ ) warrants further investigation.

The dependence of  $t_*^{(kk)}$  on the accretion, considerably dampens its sensitivity to  $N_c$  reversing our expectation (based on the analysis of  $t_0$ ) for KK to produce rain more efficiently at small  $N_c$  and less efficiently at large  $N_c$ . The weaker than expected dependency on  $N_c$  enhances the ability of relatively small dynamic differences (cloud-top heights) to compensate for microphysical differences. This interplay between auto-conversion and accretion (and the diminished role for  $N_c$ ) is not evident in the analysis of (Wood 2005), which examined each process in isolation, and in so doing may have exaggerated the role of microphysics (as represented by  $N_c$ ).

Return to our simulations in light of this analysis, Fig. 11 suggests that,

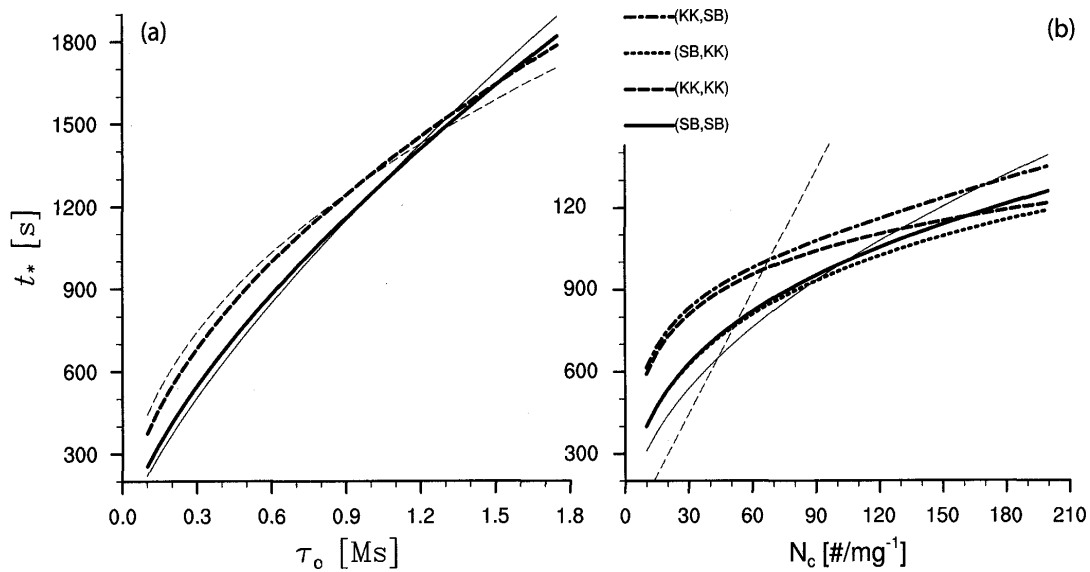


Fig. 11. Dependence of  $t_*$  rain onset time, for SB and KK schemes as a function of external parameters: (a)  $\tau_c$ , with  $N_c = 70 \text{ mg}^{-1}$ ; (b) a  $N_c$  with  $\tau_c = 0.4 \text{ Ms}$ . Calculation of  $t_*$  by integrating (23) is given by dark lines. In panel (b) we also show results with accretion schemes interchanged. Gray lines show  $0.283t_0^{(sb)}$  and  $0.168t_0^{(kk)}$  with prefactors chosen to match the mean value in left panel only for the first two integrations.

$$t_*^{(kk)}|_{N_c=35} \approx t_*^{(sb)}|_{N_c=70} \quad \text{and} \quad t_*^{(kk)}|_{N_c=70} \approx t_*^{(sb)}|_{N_c=105}.$$

This is consistent with the tendency of the KK simulations to transition to rain at droplet mixing ratios between 35 and  $70 \text{ mg}^{-1}$  while the SB simulations transition to substantial rain at mixing ratios between 70 and  $105 \text{ mg}^{-1}$ . Also, from Fig. 4 it is apparent that the SB simulation with  $N_c = 35 \text{ mg}^{-1}$  transitions to rain at about 10 hours, when clouds reach a depth just less than 2 km, while the transition to rain for the simulation with  $N_c = 70 \text{ mg}^{-1}$  occurs six hours later, only after clouds have reached a depth of about 2.2 km. Given the simplicity of the model (i.e., Eq. 23) the relevance of  $t_*$  to this transition is remarkable, as it predicts  $t_*^{(sb)} \approx 700 \text{ s}$  for  $N_c = 70 \text{ mg}^{-1}$  which given an average  $w$  of about  $2 \text{ ms}^{-1}$  corresponds to a cloud top of around 2 km, while  $t_*^{(sb)} \approx 850 \text{ s}$  for  $N_c = 35 \text{ mg}^{-1}$ , which implies that cloud tops must deepen to about 2.3 km before significant precipitation is expected to develop. Finally, we note that the tendency of the KK scheme to shut-down rain production more effectively as  $N_c$  increases (as shown in Table 3) is consistent with the  $\partial t_*^{(kk)} / \partial N_c > \partial t_*^{(sb)} / \partial N_c$  for a given  $t_*$ . Overall we find the ability of the simple model to rationalize the simulations quite satisfactory.

### c. Self-collection and break-up

In Section 3 we argued that self-collection is important based on the fact that the SB representation of it led to non-trivial changes in the simulation. Such a result would also follow if the self-collection representation was too active. To examine this issue further it proves useful to examine the histogram of the surface rain rate as function of rain rate intensity, which is plotted in Fig. 12. The figure shows that the neglect of self collection leads to a dearth of large drops. This behavior appears difficult to justify, particularly given that the basic process of self-collection is not in doubt. These data also suggests a way to use data to help constrain the modeling of this process.

Including a representation of drop break-up (S11) does lead to marginal changes in the simulation, but does not significantly change the histogram of surface rain rates (relative to S03). Hence to the extent drops are becoming large enough to start breaking up, they are apparently not critical to determining the shape of the histogram of rain-rate intensities.

## 5. Summary

Large-eddy simulation of shallow precipitating cumulus have been used to explore the sensitivity of the macroscopic cloud structure to uncertain choices in their microphysical representation. The

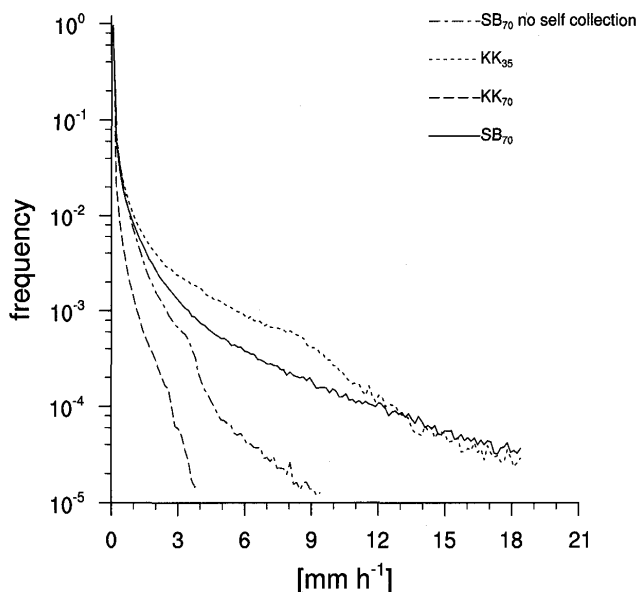


Fig. 12. Histograms showing frequency of surface rain rate as a function of intensity. Legends subscript give droplet concentrations and lines refer to simulations S06, S08 (with  $N_c = 35 \text{ mg}^{-1}$ ), S08, and S01 from top to bottom respectively.

behavior of the simulations has been interpreted with the help of simpler microphysical models, including an idealized rain-shaft model and a parcel model. Both provide useful insight into how the simulations would respond to changes in their microphysical representation, and the dominant microphysical interactions operative, in at least simulations of, shallow convection.

Our analysis suggests that unlike for stratocumulus, the microphysical representation of shallow cumulus convection requires the representation of the full suite of warm-phase microphysical processes, as effects such as self-collection of rain drops, and their break-up, can be significant. The shape of the rain-drop spectrum, at least in so far as it deviates (or is narrower) than an exponential distribution, is shown to be important for the representation of sedimentation, as too broad a distribution too readily moves rain to the surface, and stunts the development of the clouds.

We find that representing the rain-drop spectrum as an exponential distribution unrealistically distorts the sedimentation process in a way that impacts the simulations as a whole. However, as long as some means for maintaining a narrower rain-drop distribution is devised, the simulations do not appear to be sensitive to the details by which this

is accomplished, for instance differences between simulations assuming a gamma-distribution shape parameter of five, or ten, are small, nor do more sophisticated relationships between this shape parameter and the other moments of the distribution noticeably change the behavior of the simulations.

Regardless of which microphysical scheme we use there is a significant dependence of rain rate on number concentration. However, this dependence is not continuous, i.e., rain rate does not scale with cloud-droplet concentrations. Both simple models, and the simulations suggest that to a first approximation the number concentration simply selects the cloud depth at which rain will become active, with different schemes predicting different critical cloud depths. The relationship between this critical depth and the number concentration is continuous, but depends less strongly on number concentration than would be predicted by an analysis of the representation of auto-conversion process alone (cf., Wood 2005).

Physically, in cases when precipitation is the principal brake on cloud growth (see Stevens 2007b) this suggests that changes in the ambient aerosol will simply act to delay the onset of precipitation. However, because the dependence of precipitation development on cloud-droplet number concentrations is much weaker than it is on cloud liquid-water content, even the doubling of aerosol number concentrations may be offset by rather small dynamical differences. As a result clouds with greater aerosol loadings may develop rain later in the evolution of the cloud layer, but when they do they may well rain more heavily.

A corollary of this finding is that because environmental factors (the humidity of the cloud layer) and model choices (resolution) can determine whether or not a particular simulation crosses this threshold, precipitation development in and among simulations can be both physically and numerically delicate.

### Acknowledgement

L. Nuijens, A.P. Siebesma, M.C. van Zanten and the rest of the GCSS boundary layer clouds working group are thanked for their help in setting up the RICO case study upon which much of our analysis is based. NCAR is thanked for providing computational resources for the simulations, and for hosting both authors during the initial stages of this investigation. Two anonymous reviewers are thanked for their unusually thorough and construc-

tive reviews which led to substantial improvements in the manuscript. In addition the first author would like to thank R. Klein, P. Deufelhard and the Konrad-Zuse-Zentrum für Informationstechnik in Berlin, which hosted him during the period in which this work matured. Financial support has been provided by NSF Grant ATM-0336849 and through the Center for Multiscale Modeling of Atmospheric Processes. Lastly, the presentation of these ideas at the International workshop on high-resolution observations and & cloud modeling, to which this special issue is devoted, stimulated their development.

### Appendix

#### Numerical implementation of microphysical scheme

##### a. Sedimentation

To numerically represent the sedimentation in the model we use a flux-form Semi-Lagrangian scheme. This yields stable solutions even for Courant (CFL) numbers greater than one. The basic algorithm solves the sedimentation equation (22) where  $\psi$  denotes the microphysical variable (in our case either  $n_r$  or  $r_r$ ) and  $w_\psi$  is given by (13) and (14). Because  $w_\psi$  is bounded at  $w_{mx} = 9.65 \text{ m s}^{-1}$  the maximum CFL number is known *a priori* and is given by

$$C_{mx} = \frac{w_{mx} \Delta t}{(\Delta z)_{\min}}, \tag{30}$$

where  $\Delta t$  denotes the model time step and  $(\Delta z)_{\min}$  is the minimum vertical grid increment in the model. Because of size sorting, one can expect the threshold velocity  $w_{mx}$  to be realized frequently in a simulation, hence  $C_{mx}$  is a practical as well as theoretical upper bound.

The scheme we use is based on a modified upwind approach where the velocity in grid cell  $l$  is defined as

$$V_{\psi,l} = \frac{1}{4}(w_{\psi,l-1} + 2w_{\psi,l} + w_{\psi,l+1}), \tag{31}$$

where here  $l$  denotes the grid level. This velocity is defined using the three-point stencil  $(l - 1, l, l + 1)$  so as to better represent the mean velocity of the drops within a cell in situations when all of the mass within a cell is expected to move through the cell interface. It is used to define the local Courant

number for that cell

$$C_{\psi,l} = \frac{V_{\psi,l} \Delta t}{\Delta_l z}, \tag{32}$$

where  $\Delta z$  is the cell thickness. The flux at the cell interface, is then given by

$$F_{l-1/2} = \frac{1}{\Delta t} \sum_{l' \in \ell} \max(1, C_{k,l'} - (l' - l)) \tilde{\psi}_{l'} \Delta z, \tag{33}$$

where  $\ell$  defines the set of continuous  $l' > l$  for which

$$C_{k,l'} > (l' - l), \tag{34}$$

and  $\tilde{\psi}_{l'}$  is the effective concentration of the over that fraction of the  $l'$  cell which passes through the  $l - 1/2$  cell interface through the course of a time-step. For a low order scheme  $\tilde{\psi}_{l'} = \psi_{l'}$  corresponds to the upwind approximation. We use a slope limited higher order scheme for which

$$\tilde{\psi}_{l'} = \psi_{l'} - \frac{d\psi_{l'}}{dz} \left( 1 - \frac{\delta z}{\Delta z} \right) \frac{\Delta z}{2}, \tag{35}$$

where the slopes  $\frac{d\psi_{l'}}{dz}$  are estimated based on the neighboring grid cells, and limited to insure monotonicity. The quantity  $\delta z / \Delta z$  is just the adjusted Courant number, i.e., that fraction of the cell  $l'$  which passes through the  $l - 1/2$  interface within a time step. In practice the scheme is also generalized to account for variable grid spacings, and the summation over  $l'$  is implemented through the use of a *do while* statement. Once the fluxes are defined on cell-interfaces, the tendency due to sedimentation is simply calculated as

$$\frac{\partial \psi}{\partial t} \Big|_l = - \frac{F_{\psi,l+1/2} - F_{\psi,l-1/2}}{\Delta_l z}. \tag{36}$$

We find that the scheme does reasonably well for  $C_{mx} < 2$ . Configurations resulting in a larger value of  $C_{mx}$  imply that mass is moving through at least two intermediate cells before arriving at its final location. Because such sedimentation happens without the possibility of microphysical or thermodynamic interactions with the intervening media, choosing time steps so large as to make  $C_{mx} > 3$  is probably unwise. This places a practical limit on the time step for the scheme as

$$\Delta t \leq \frac{2w_{mx}}{(\Delta z)_{\min}}, \quad (37)$$

which is readily met in our simulations as  $\Delta t$  is generally less than 2 s. For schemes whose dynamical time step is much greater than this, the parameterized processes (turbulence, microphysics, etc) should be sub-cycled so as to maintain the above time step constraint. As a practical matter, sedimentation is time split from the rest of the code so as to ensure the stability constraints motivating the above description are satisfied (i.e., this allows us to neglect the local flow velocity when estimating  $C_{mx}$  for sedimentation).

#### b. Numerical issues

Both transport and advection processes can produce arbitrarily large drops, and unrealistic concentrations. The monotone nature of transport assures positivity of  $n_r$  and  $r_r$  in the absence of other processes. However the accumulation of tendencies from multiple processes can generate negative values of  $n_r$  and  $r_r$ . To address this issue we set  $r_r = \max(0, r_r)$  before and after the call to the microphysical routines, at these times we also adjust  $n_r$  to maintain  $2 \mu\text{m} < D_m < 1 \text{ mm}$ .

### References

- Ackerman, A.S., M.P. Kirkpatrick, D.E. Stevens, and O.B. Toon, 2004: The impact of humidity above stratiform clouds on indirect aerosol climate forcing. *Nature*, **432**, 1014–1017.
- Baldauf, M., K. Stephan, S. Klink, C. Schraff, A. Seifert, J. Förstner, T. Reinhardt, and C.-J. Lenz, 2007: The new very short range forecast model COSMO-LMK for the convection resolving scale. Technical report, Deutscher Wetterdienst, Kaiserleistr. 42, 63067 Offenbach Germany, available from michael.baldauf@dwd.de.
- Chen, C. and W.R. Cotton, 1987: The physics of the marine stratocumulus-capped mixed layer. *J. Atmos. Sci.*, **44**, 2951–2977.
- Cotton, W.R., 1972: Numerical simulation of precipitation development in supercooled cumuli-part I. *Mon. Wea. Rev.*, **100**, 757–763.
- Feingold, G., R.L. Walko, B. Stevens, and W.R. Cotton, 1994: Simulations of marine stratocumulus using a new microphysical parameterization scheme. *Atmos. Res.*, **47–48**, 505–528.
- Jiang, H. and W.R. Cotton, 2000: Large-eddy simulation of shallow cumulus convection during bomex: Sensitivity to microphysics and radiation. *J. Atmos. Sci.*, **57**, 582–594.
- Khairoutdinov, M.F. and Y.L. Kogan, 2000: A new cloud physics scheme in a large-eddy simulation model of marine stratocumulus. *Mon. Wea. Rev.*, **128**, 229–243.
- Kogan, Y.L., M.P. Khairoutdinov, D.K. Lilly, Z.N. Kogan, and Q. Liu, 1995: Modeling of stratocumulus cloud layers in a large eddy simulation model with explicit microphysics. *J. Atmos. Sci.*, **52**, 2293–2940.
- Larson, V.E., R. Wood, P.R. Field, J.-C. Golaz, T.H.V. Haar, and W.R. Cotton, 2001: Systematic biases in the microphysics and thermodynamics of numerical models that ignore subgrid-scale variability. *J. Atmos. Sci.*, **58**, 1117–1128.
- Long, A.B., 1974: Solutions to the droplet coalescence equation for polynomial kernels. *J. Atmos. Sci.*, **31**, 1040.
- Lüpkes, C., K.D. Beheng, and G. Doms, 1989: A parameterization scheme simulating warm rain formation due to collision/coalescence of water drops. *Contributions to Atmospheric Physics*, **62**, 289–306.
- Marshall, J. and W. Palmer, 1948: The distribution of raindrops with size. *J. Meteor.*, **5**, 195–166.
- Milbrandt, J.A. and M. Yau, 2005: A multimoment bulk microphysics parameterization. part I: analysis of the role of the spectral shape parameter. *J. Atmos. Sci.*, **62**, 3051–3064.
- Morrisson, H. and W.W. Grabowski, 2007: Comparison of bulk and bin warm rain microphysics using a kinematic framework. *J. Atmos. Sci.*, **64**, 2839–2861.
- Rauber, R., B. Stevens, H.T. Ochs III, C. Knight, B.A. Albrecht, A. Blyth, C. Fairall, J.B. Jensen, S.G. Lasher-Trapp, O.L. Mayol-Bracero, G. Vali, J.R. Anderson, B.A. Baker, A.R. Bandy, F. Burnet, J.-L. Brenguier, W.A. Brewer, P.R.A. Brown, P. Chuang, W.R. Cotton, L.D. Girolamo, B. Geerts, H. Gerber, S. Göke, L. Gomes, B.G. Heikes, J.G. Hudson, P. Kollias, R.P. Lawson, S.K. Krueger, D.H. Lenschow, L. Nuijens, D.W. O'Sullivan, R.A. Rilling, D.C. Rogers, A.P. Siebesma, E. Snodgrass, J.L. Stith, D. Thornton, S. Tucker, C.H. Twohy, and P. Zuidema, 2007: Rain in (shallow) cumulus over the ocean—the RICO campaign. *Bull. Amer. Meteor. Soc.*, **88**, 1912–1928.
- Savic-Jovicic, V. and B. Stevens, 2008: The structure and mesoscale organization of precipitating stratocumulus. *J. Atmos. Sci.*, **65**, 1587–1605.
- Seifert, A., 2008: On the parameterization of evaporation of raindrops as simulated by a one-dimensional rainshaft model. *J. Atmos. Sci.*, (in press).
- Seifert, A. and K.D. Beheng, 2001: A double-moment parameterization for simulating autoconversion, accretion and self collection. *Atmos. Res.*, **59–60**, 265–281.
- Siebesma, A.P., C.S.B.A. Brown, A. Chlond, J. Cuxart,

- P. Duynkerke, H. Jiang, M. Khairoutdinov, D. Lewellen, C.-H. Moeng, E. Sanchez, B. Stevens, and D.E. Steven, 2003: A large-eddy simulation study of shallow cumulus convection. *J. Atmos. Sci.*, **60**, 1201–1219.
- Stevens, B., 2007: On the growth of layers of non-precipitating cumulus convection. *J. Atmos. Sci.*, **64**, 2916–2931.
- Stevens, B., W.R. Cotton, G. Feingold, and C.-H. Moeng, 1998: Large-eddy simulations of strongly precipitating, shallow, stratocumulus-topped boundary layers. *J. Atmos. Sci.*, **55**, 3616–3638.
- Stevens, B., C.-H. Moeng, A.S. Ackerman, C.S. Bretherton, A. Chlond, S. de Roode, J. Edwards, J.-C. Golaz, H. Jiang, M. Khairoutdinov, M.P. Kirkpatrick, D.C. Lewellen, A. Lock, F. Müller, D.E. Stevens, E. Whelan, and P. Zhu, 2005: Evaluation of large-eddy simulations via observations of nocturnal marine stratocumulus. *Mon. Wea. Rev.*, **133**, 1443–1462.
- Tomita, H., H. Miura, S. Iga, T. Nasuno, and M. Satoh, 2005: A global cloud-resolving simulation: preliminary results from an aqua planet. *Geophys. Res. Lett.*, **32**, doi:10.1029/2005GL022459.
- Wacker, U. and A. Seifert, 2001: Evolution of rain water profiles resulting from pure sedimentation: Spectral vs. parameterized description. *Atmos. Res.*, **58**, 19–39.
- Wood, R., 2005: Drizzle in stratiform boundary layer clouds. Part II: microphysical aspects. *J. Atmos. Sci.*, **62**, 3034–3046.
- Xue, H., G. Feingold, and B. Stevens, 2008: Aerosol effects on clouds, precipitation, and the organization of shallow cumulus convection. *J. Atmos. Sci.*, **65**, 392–406.